Carrier Decay and Diffusion Dynamics in Single-Crystalline CdTe as Seen via Microphotoluminescence

B. Fluegel,[1][*] K. Alberi,[1] M. J. DiNezza,[2] S. Liu,[2] Y.-H. Zhang,[2] and A. Mascarenhas[1]

[1]*National Renewable Energy Laboratory, 15013 Denver West Boulevard, Golden, Colorado 80401, USA*
[2]*Center for Photonics Innovation and School of Electrical, Computer and Energy Engineering,*
Arizona State University, Tempe, Arizona 85287, USA
(Received 4 June 2014; published 24 September 2014)

The ability to spatially resolve the degree to which extended defects impact carrier diffusion lengths and lifetimes is important for determining upper limits for defect densities in semiconductor devices. We show that a new spatially and temporally resolved photoluminescence (PL) imaging technique can be used to accurately extract carrier lifetime values in the immediate vicinity of dark-line defects in CdTe/MgCdTe double heterostructures. A series of PL images captured during the decay process show that extended defects with a density of 1.4×10^5 cm^{-2} deplete photogenerated charge carriers from the surrounding semiconductor material on a nanosecond time scale. The technique makes it possible to elucidate the interplay between nonradiative carrier recombination and carrier diffusion and reveals that they both combine to degrade the PL intensity over a fractional area that is much larger than the physical size of the defects. Carrier lifetimes are correctly determined from numerical simulations of the decay behavior by taking these two effects into account. Our study demonstrates that it is crucial to measure and account for the influence of local defects in the measurement of carrier lifetime and diffusion, which are key transport parameters for the design and modeling of advanced solar-cell and light-emitting devices.

I. INTRODUCTION

The use of new semiconductor materials, heterostructures, and large-scale deposition techniques for optoelectronic device design and fabrication increasingly requires careful control of defect formation. Crystalline defects in bulk and quantum-confined semiconductors often act as regions of strong nonradiative carrier recombination [1,2] and can detrimentally alter the spatially averaged carrier densities that are photogenerated in solar cells [3] or electrically injected in light-emitting devices [4]. It is, therefore, essential to be able to experimentally probe the extent to which defects locally influence carrier lifetimes and diffusion lengths in order to understand their overall effect on device performance. Despite this importance, the dynamics of recombination processes is usually determined only indirectly. The influence of microscopic and uniformly distributed nonradiative recombination sites is typically analyzed statistically through spatially averaged measurements of photoluminescence (PL) [5], absorption [6], or transient grating [6] lifetimes. Extended defects, such as dislocations and grain boundaries, are more difficult to properly evaluate. Photoluminescence and cathodoluminescence (CL) mapping techniques are routinely used to spatially resolve regions of higher nonradiative recombination associated with these defects [7–9]. Temporally resolved PL or absorption mapping techniques

have also been used on occasion to determine the localized effects of grain boundaries [10] and stacking faults [11] on carrier lifetimes. However, lower carrier densities in the region immediately surrounding a defect arise from an equilibrium between carrier recombination and diffusion. The interrelated dynamics of these two processes, therefore, make it impossible to simply extract carrier lifetimes from PL decay curves obtained from time-resolved PL mapping measurements performed with a point source. New techniques that simultaneously spatially and temporally resolve the motion of carriers at, near, and far from isolated defects will make it possible to precisely determine the exact values of carrier transport parameters that critically influence the design of solar-cell and light-emitting devices.

In this work, we present a new spatially and temporally resolved PL imaging technique that allows us to separate the dynamics of carrier decay and diffusion in order to accurately extract the intrinsic carrier lifetime near individual extended defects. Measurements are performed on MBE-grown single-crystalline CdTe/MgCdTe double heterostructures (DHs) that exhibit dark-line defects of reduced PL intensity associated with dislocations or twins. A series of 2D images captured on an intensified gated CCD with ns time resolution immediately after excitation directly show that carrier diffusion into the depleted region surrounding extended defects profoundly influences the spatial extent to which the defect affects carrier recombination. We show that both nonradiative carrier

[*]brian.fluegel@nrel.gov

recombination and carrier diffusion toward these defects must be taken into account to extract the true effects of these defects on the carrier lifetimes in these materials. The development of such a characterization technique and set of measurement guidelines will significantly advance methods for characterizing semiconductor material in order to correlate with optoelectronic-device performance.

II. EXPERIMENT

A CdTe/MgCdTe DH grown on an InSb substrate in a dual-chamber MBE is designed in order to study CdTe with substantially reduced surface and interface recombination [12]. The results show that the 1-μm-thick active layer is coherently strained to the substrate and exhibits high room-temperature PL intensity and lifetime [12]. In the present work, the DH is placed in a liquid-nitrogen cryostat at the object plane of a 0.7 numerical-aperture objective. Excitation is from a sub-ps mode-locked Ti:sapphire laser. In order to selectively excite into the DH active layer and to simplify the carrier generation dynamics, the laser energy is tuned to 1.62 eV, just above the CdTe band-gap energy. The laser can be either focused through the objective lens to a 0.8-μm spot or defocused to a beam with a diameter larger than the 240-μm field in order to uniformly illuminate the sample. Discrete edge filters are used to reject laser scatter at energies above 1.58 eV while selecting the PL spectral band of interest, and the 2D field of PL is imaged onto an intensified gated CCD camera with a 2-ns time resolution. For higher temporal resolution, a 1D line from the field is projected onto a streak camera set to 0.5-ns resolution. The laser repetition rate is 2 MHz for the streak camera or 500 kHz for the CCD. The pulse fluence is kept lower for the wide-field excitation in order to prevent sample heating. Under these conditions, no evidence of sample degradation is observed, and the PL characteristics are constant over measurement times of 10^3 s.

III. RESULTS

The 80-K PL spectrum of the CdTe DH shown in Fig. 1 is comparable to those that have been previously published for polycrystalline [13] and single-crystalline CdTe [14]. This spectrum is obtained with a cw laser at 2.3 eV in order to show the full spectral region around the band edge. However, the PL spectra obtained with the pulsed laser centered at 1.62 eV, which is used for all subsequent imaging and time-resolved measurements, exhibit similar features. The full spectrum contains a bound exciton peak at 1.58 eV near the direct band gap and a much wider phonon-broadened band extending over the range of 1.3–1.5 eV. The results below refer to these as exciton and low-energy PL bands, respectively.

Figure 2 shows a time-integrated PL (TIPL) 2D image generated under wide-field pulsed excitation by detecting both of the spectral bands with the Si CCD. The image
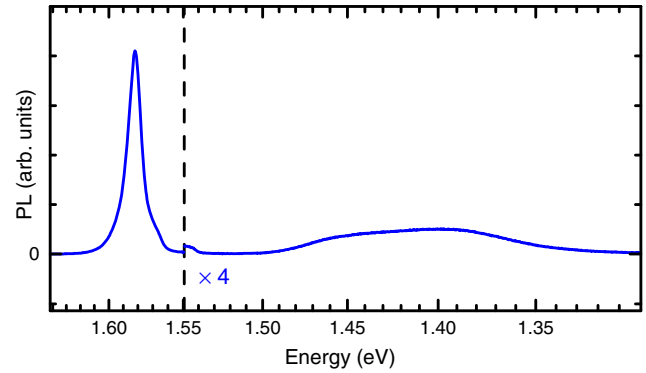

FIG. 1. 80-K PL spectrum under 2.3-eV excitation of 45 W/cm². The vertical axis is expanded for the region of the low-energy band.
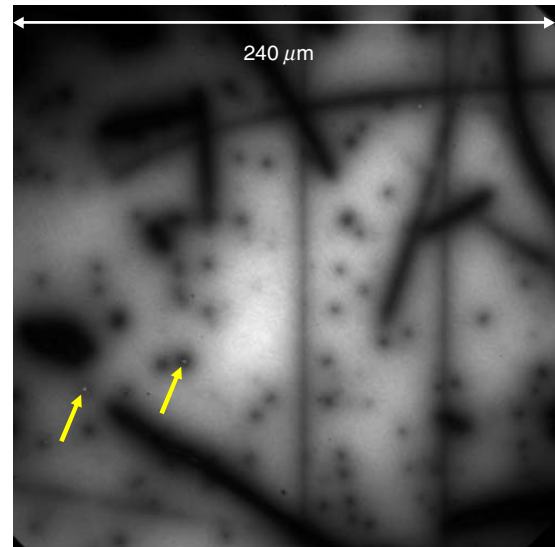

FIG. 2. Time-integrated PL image under 700 nJ/cm² pulsed wide-field illumination filtered to pass both spectral bands. Bright points of low-energy PL are seen in the centers of some dark spots (arrows), indicating the system spatial resolution.

shows a complex pattern of dark-line defects across the field. The density of the dotlike features is 1.4×10^5 cm^{-2}. Several of these dots indicated by the arrows contain bright features at their centers that emit within the low-energy band. The spatially broad extended lines, 4 to 8 μm wide, are similar to those seen in CL images of single-crystal CdTe (Ref. [9]). The dark lines and the bright regions surrounding them are dominated by emission at the exciton band. A significant fraction of the image area has degraded PL efficiency due to the darker regions.

The poor spatial definition of these dark-line defects compared to the sharp low-energy points indicates that carrier diffusion influences the spatial distribution of radiative recombination from the exciton band. This insight is confirmed by the time-resolved PL data obtained by imaging the PL data onto a streak camera. The inset to
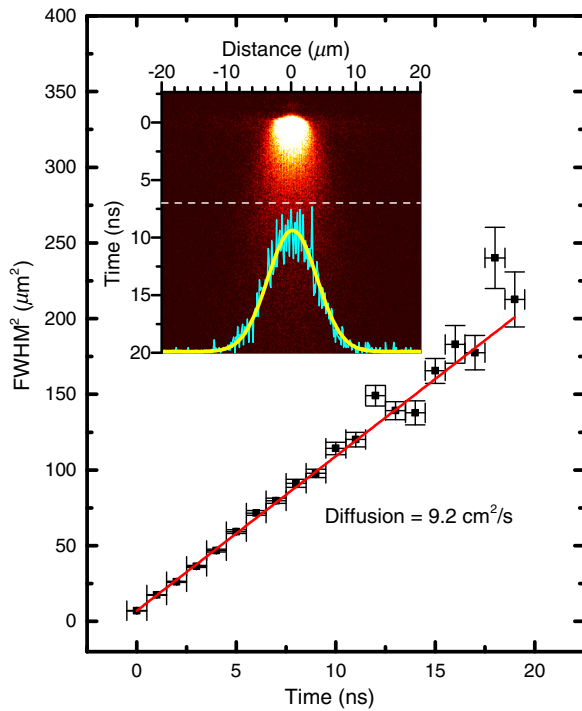
FIG. 3. The squared FWHM of the Gaussian fit to the exciton PL profile as a function of time after excitation by a 3 $\mu J/cm^2$ focused pulsed laser. Points are measured widths; solid line is a linear fit to points. Inset: Streak camera trace from which the spatial profiles are extracted at 1-ns intervals. Solid curves show the profile through the dashed line at 7 ns and its Gaussian fit.
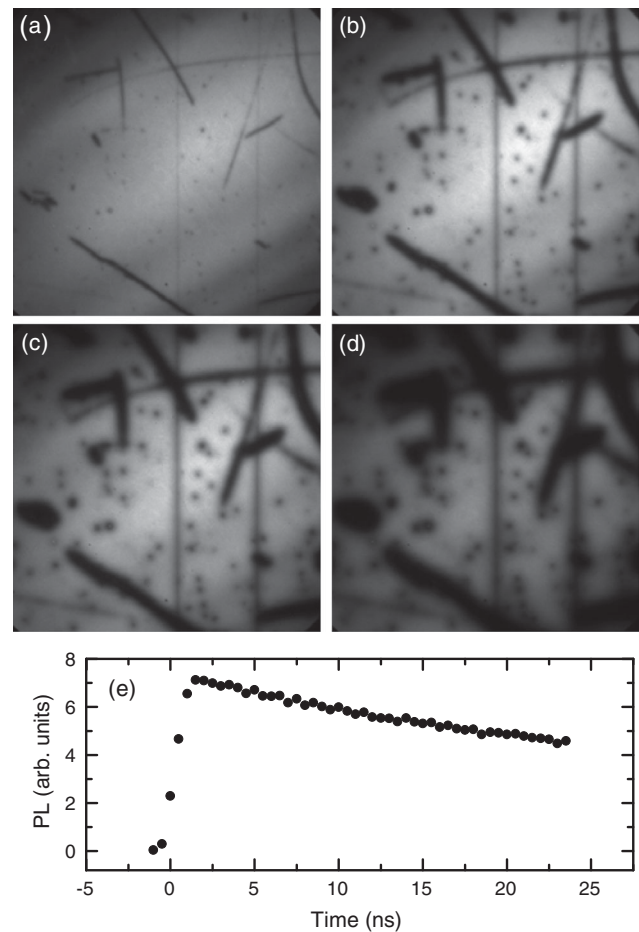

FIG. 4. Time-resolved PL maps of the exciton PL taken 0.5 ns (a), 5 ns (b), 10 ns (c), and 25.5 ns (d) after the laser pulse. Excitation conditions and sample region are identical to Fig. 2. (e) Spatially integrated PL in a 15-μm-wide bright region as a function of time for the full data set.

Fig. 3 shows a streak camera trace from a region of the sample selected far from any dark-line defects and excited by a focused laser beam. The PL decay of this single-crystal CdTe sample is much slower than the exciton PL lifetime measured in polycrystalline CdTe [13]. Excitonic PL is also emitted from an area that is larger than the laser spot and which grows even larger with time, clearly indicating lateral diffusion.

Carrier diffusion from a point excitation source and within depletion regions will have a strong effect on any attempt to measure lifetime in these dark regions. To quantify this effect, we measure the spatial profile of the diffusing PL spot as a function of time. The profile for one selected time and the Gaussian fit are shown in the Fig. 3 inset. For a Gaussian-shaped laser focus, this time-dependent PL profile has an analytical solution [15,16] which allows the diffusion coefficient to be extracted by plotting the square of the PL profile full width at half maximum (FWHM). Our profiles are well fit to the Gaussian shape, indicating simple diffusive motion, and the plot in Fig. 3 gives a diffusion coefficient of 9.2 cm^2/s for an excited carrier concentration of 1×10^{17} cm^{-3}.

Because the dark-line defects in Fig. 2 are apparently narrower than the extracted diffusion length, we analyze them in imaging mode, i.e., by time resolving the 2D image of Fig. 2. Figure 4(a) shows a quite different PL image

when the same region is recorded with a 2-ns gate timed at 0.5 ns relative to the wide-field laser pulse. At this time, the dark lines are initially 5–6 times narrower than those obtained by the TIPL measurement, with some lines as narrow as the microscope resolution (1.5 μm). As the camera gate is advanced from the time of the arrival of the laser pulse, the PL intensity of the bright regions increases, while the dark lines grow in thickness. This growth increases for many ns (Ref. [17]) after the laser pulse until the dark lines occupy a large portion of the field, as seen in Figs. 4(b)–4(d). The contrast of the PL intensity at the dark-line defects compared to the surrounding material is also greater for the thicker lines. The defect-free lifetime is obtained by integrating the PL over a 15-μm bright region near the center of the field. The resulting time decay is shown in Fig. 4(e) and gives a time constant of 48 ns.

The images in Fig. 4 allow us to visualize carrier diffusion in the vicinity of the dark-line defects. Since diffusion clearly plays a large role in the recombination

dynamics, we model the dark lines as regions that differ from their surroundings only in the rate of nonradiative recombination. Under spatially uniform wide-field pulsed excitation, the PL intensity will be spatially constant at $t = 0$. For $t > 0$, the fast nonradiative decay rate inherent to the defects starts to reduce the carrier density and the PL intensity in the immediate region of the defect. This is countered by the strong diffusion that draws carriers in from surrounding regions and increases the observed width of the dark-line defects far in excess of their physical manifestation in the crystal structure.

Specifically, we use a time-dependent version of the steady-state calculation in Ref. [7]. The carrier density $n(\vec{r}, t)$ is governed by

$$\frac{dn(\vec{r}, t)}{dt} = -\frac{n(\vec{r}, t)}{\tau(\vec{r})} + D\nabla^2 n(\vec{r}, t), \qquad (1)$$

where D is the diffusion coefficient, and $\tau(\vec{r})$ is the inverse of the total recombination rate. τ takes the values τ_d and τ_b in the defect and bright (defect-free) regions, respectively. For simplicity, the problem is solved in two dimensions, i.e., constant in the z direction. Furthermore, the spatially constant laser generation of carriers is considered to be much faster than other processes and is, therefore, taken as an initial condition. In order to simulate the smallest features of Fig. 4(a), we fill our 2D space with a single dark-line defect and a point defect modeled as a 2-μm-wide rectangle and a 2-μm circle, respectively. The decay and diffusion that evolve after the initial constant density are calculated by finite-element analysis. The radiative component of $\tau(\vec{r})$ is assumed to be spatially constant, and, therefore, the PL intensity is simply proportional to $n(\vec{r}, t)$.

The input parameters for the calculation are determined from the measured results above. D is set at 10 cm^2/s based on the results of Fig. 3, and τ_b is set at 50 ns to match the PL temporal decay measured in the bright regions of Fig. 4. A ratio of $\tau_b/\tau_d = 10$ is used to reproduce the measured PL contrast between the bright and dark regions. Figure 5(a) shows the simulated PL image at 1 ns after the uniform carrier generation, which indicates that accelerated recombination has reduced the PL intensity in the areas that coincide with the defect shapes. The dark areas have softened boundaries due to the effects of simultaneous carrier diffusion. The solid lines plotted through Figs. 5(a)–5(d) depict the PL intensity on a $y = 0$ cut through the two defects. The 1-ns PL intensity at the rectangle defect is approximately 90% of the surrounding area and has a FWHM of 2.4 μm, which is slightly larger than the defined defect width. The contrast is higher for the wider defect regions (modeled but not shown). Both the width and the contrast of the PL dark region increase with increasing time as seen in Figs. 5(b)–5(d) (Ref. [17]). Figure 6 shows the time dependence of the calculated PL at important locations relative to the defects. Far from the
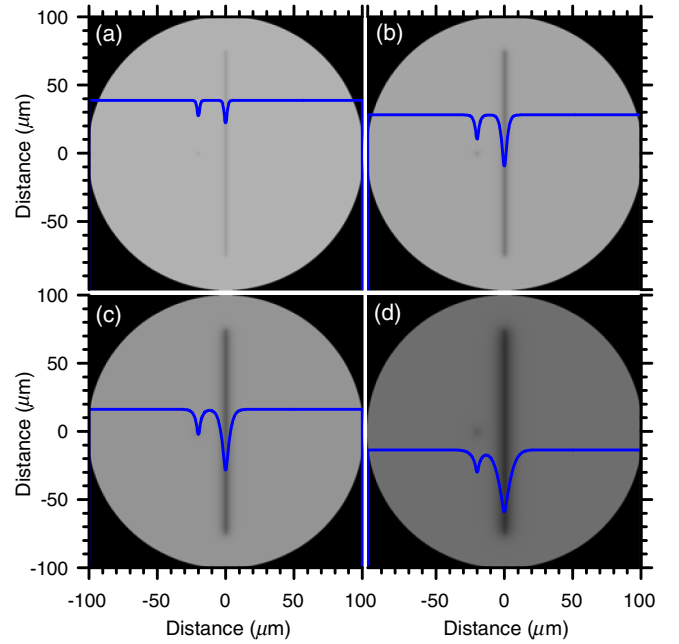

FIG. 5. Calculated PL intensities after pulsed wide-field illumination. Times are 1 ns (a), 5 ns (b), 10 ns (c), and 25 ns (d). Model defects are a 2-μm-diameter circle at $(-20, 0)$ and a 2-μm-wide wide rectangle at $(0, 0)$ μm. Solid lines are a profile of the PL along $y = 0$ drawn relative to the panel bottom.
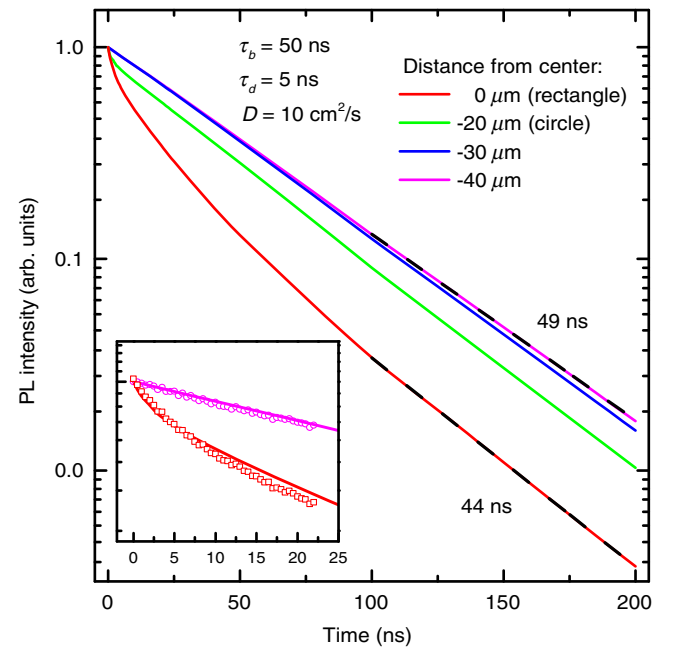

FIG. 6. Time profiles of the calculated results in Fig. 5 at points along the $y = 0$ axis. Solid lines are taken at (from top to bottom) $x = -40, -30, -20$ μm, and 0. Dashed lines are exponential fits to the region 100–200 ns yielding the time constants shown. Inset: Expanded plot of the early time region comparing the 0 and -40 μm profiles (lines) with normalized PL (symbols) from Fig. 4(e) and from a similar region of interest centered on a thin line defect.

defects (-40 μm) the decay follows a simple exponential decay given by τ_b. At the defects, the initial decay at $t = 0$ occurs at the faster rate τ_d^{-1}, but it immediately slows and eventually matches the more distant areas, which act as a source of carriers that repopulates the depleted region immediately surrounding the defects. The two regions are compared in the inset of Fig. 6, which shows close agreement between the calculated PL decay and the values measured from the bright and dark regions of Fig. 4.

As shown in the TIPL image of Fig. 2, some of the defects that appear as dark spots contain at their center bright points that emit strongly at the low-energy PL band. These bright features have also been observed in CL at the line-shaped defects [9]. PL emission at similar energies has been observed in polycrystalline CdTe and corresponds to radiative recombination from deep impurity states that participate in carrier diffusion at low temperature [13]. The TI image of Fig. 7(a) shows that a bright point emitter can be detected even when the pulsed laser illumination is not uniform but rather focused to a location 20 μm to its right. Both spectral bands are detected in this image, and the PL at the excitation spot is 15 times brighter than the point emitter, rendering the main figure saturated at the point of the laser. A rescaled image is shown in the inset of Fig. 7(a), and the effect of diffusion can be seen in its size and shape. Unlike Fig. 3, this is a steady-state measurement with a high-repetition-rate laser approximating a constant generation rate. The tails of its PL spot are, therefore, significantly wider than a Gaussian profile, as expected from the analytical solution to this problem [18].

Figure 7(a) indicates that the bright point can capture carriers and allow them to radiatively recombine much more efficiently than the material in the region between it and the excitation location. The TRPL in the vicinity of the laser is dominated by the same diffusing band-edge component that is seen in the defect-free material (Fig. 3, inset). However, the capture of the band-edge carriers into low-energy states at the bright point can be directly observed. Figure 7(b) shows a streak camera trace at the same location and under the same conditions as Fig. 7(a) but masked at the excitation spot to block the intense PL there. Beyond the mask, exciton PL from diffusing carriers is observed to expand to the left. The rise of the PL emission at the bright spot occurs approximately 13 ns after the laser pulse, which coincides with the expansion of carriers emitting at the exciton band. Spectral measurements confirm that the bright point's PL is composed of the low-energy band. This measurement allows us to directly image the existence of long carrier-diffusion lengths within the material.

IV. DISCUSSION

The PL spectrum of this undoped MBE-grown CeTe/MgCdTe DH sample can be compared with studies of undoped melt-grown bulk CdTe having impurity concentrations in the range of 10^{17} cm^{-3} (Ref. [14]). In those materials, neutral acceptor bound exciton and the donor-acceptor pair PL bands originate from partially compensated acceptors [19]. The exciton PL and low-energy PL from the present sample correspond closely in energy to those bands. Given the large acceptor localization energy of 146 meV, we expect that the present MBE-grown sample will have a free carrier concentration much less than the photogenerated concentrations of 10^{16}–10^{18} cm^{-3}. The diffusion measured here will, therefore, be ambipolar rather than a minority carrier. The photogenerated carriers diffusing through defect-free regions form into bound excitons and recombine at acceptors. The defect regions, in addition to being nonradiative recombination centers as postulated in our model, may also change the dominant radiative recombination mechanism, resulting in the bright emission of low-energy PL seen from the center of the dark lines (Fig. 2, arrows).

Previous measurements of single-crystal CdTe PL efficiency reveal the strong effects caused by diffusion in the vertical direction. Depth-resolved PL lifetime measurements [20,21] show that carrier lifetime is greatly increased a few microns below the surface because of reduced surface recombination. Similarly, the double heterostructure used here has previously been shown to increase PL lifetime due to carriers being separated from the surface [12]. The microscopy results presented here can, therefore, be attributed to lateral diffusion within the CdTe layer. The defect-free lifetime obtained from Fig. 4(e), combined with the diffusion constant obtained from Fig. 3, gives a rather long diffusion length of 6 μm. Carriers, therefore, diffuse into depleted regions surrounding the defect. If this diffusion is not accounted for when extracting PL lifetimes from spatially resolved PL measurements, the values will be inaccurate. Diffusion, therefore, complicates standard
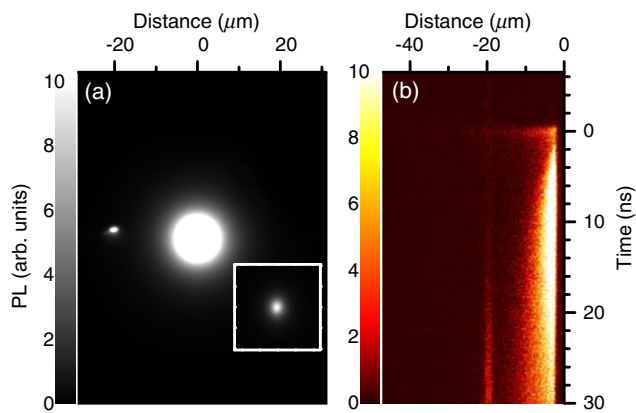

FIG. 7. (a) Time-integrated image of both PL spectral bands under focused pulsed excitation at $(0, 0)$ μm, taken in a sample region that contains a bright point emitter at $(-21, 0)$ μm. Inset: The same data on a rescaled gray scale map to correctly show the excitation point profile more clearly. Spatial scales are unchanged. (b) Streak camera trace of the same signal in (a).

approaches to measuring and understanding the material performance in single-crystal CdTe. Using uniform illumination with imaged detection, τ_b can be accurately estimated in a region sufficiently far from defects, as in Fig. 4(e). However, the recombination lifetime of the region immediately surrounding the numerous dark-line defects will be overestimated even in 1D or 2D TRPL measurements that are capable of spatially resolving them. Our estimate of 5-ns carrier lifetimes in the vicinity of the defects, obtained from comparison with the calculation, is much faster than the surrounding defect-free areas. As Fig. 6 shows, this rapid decay can be observed only near $t = 0$. The correct analysis to extract lifetimes that spatially vary over distances smaller than the diffusion length is to treat decay and diffusion as coupled phenomena, as shown in Fig. 5. The good agreement between our experimental and calculated images (Figs. 4 and 5) showing the temporal growth of dark-line defects, both in width and in contrast, indicates that our simulation of the coupled decay and diffusion is accurate and useful. The calculation can also be used to evaluate alternative possibilities, such as that the dark-line defects may have physical characteristics other than just nonradiative recombination which help explain their darker PL. Lower radiative recombination rates or initial carrier concentrations at the defects are investigated but are found to produce dynamics in disagreement with the measurement.

The total area of the spatially disjoint dark-line defects in Fig. 4(a) is only 4% of the field. The effect these defects will have on the sample-averaged carrier density can be estimated by integrating Eq. (1) over space to yield the decay of the total carrier population N,

$$\frac{dN(t)}{dt} = -\frac{N(t)}{\tilde{\tau}(t)}, \tag{2}$$

where the effective recombination rate

$$\tilde{\tau}(t)^{-1} = \int \frac{n(\vec{r}, t)}{\tau(\vec{r})} d^3r / N(t) \tag{3}$$

is a spatial average of the recombination rate weighted by the local carrier concentration. This value can be measured from the decay of the PL spatially integrated over the entire field in Fig. 4. Using the full time set as in Fig. 4(e), an approximately exponential decay is found with a lifetime of 23 ns. The small fraction of sample occupied by the defects, thus, results in an average lifetime that is half the intrinsic value of 48 ns.

This spatially and time-resolved PL imaging technique and analysis will be particularly useful in determining how processing parameters affect carrier transport in various semiconductor device layers. For example, measurements can be performed on CdTe/MgCdTe double heterostructures as a function of growth conditions and postgrowth passivation treatments to determine the best processing conditions for fabricating single-crystalline CdTe solar cells and detectors. Since longer diffusion lengths result in broadened regions of lower luminescence efficiency surrounding defects, this increases the importance of properly accounting for diffusion when spatially resolving the lifetime.

In conclusion, we demonstrate a new technique for accurately measuring carrier lifetimes in the vicinity of crystalline defects. Time-resolved PL images of dark-line defects in MBE-grown CdTe DHs show that nonradiative carrier recombination and carrier diffusion contribute to the wide depletion regions surrounding the defects. Because of the large diffusion length, 6 μm, these defects can sink carriers from a much larger volume of material, and, thus, will also affect the measurement of carrier lifetimes in this region. Extraction of the correct carrier lifetimes in the immediate vicinity of the defects requires that carriers be generated uniformly over a wide area of the sample and that the decay is numerically simulated by taking carrier diffusion into account. Using this technique, the carrier decay time in the vicinity of dark-line defects is found to be an order of magnitude faster than in the surrounding material. By directly demonstrating the interplay of carrier recombination and diffusion processes on the manifestation of the dark-line defects in PL, we demonstrate that it is crucial to measure and account for carrier diffusion when using PL imaging techniques to evaluate material performance, since the material systems with the longest diffusion lengths are the most susceptible to degradation by a low concentration of defects. Our new measurement technique provides a more straightforward and direct approach for determining how extended defects control carrier diffusion lengths and lifetimes, which are key transport parameters important for the design and modeling of optoelectronic devices such as solar cells and light-emitting devices.

[1] Y. Ohizumi, T. Tsuruoka, and S. Ushioda, Formation of misfit dislocations in GaAs/InGaAs multiquantum wells observed by photoluminescence microscopy, J. Appl. Phys. **92**, 2385 (2002).

[2] K. Okamoto, S. Fujita, Y. Kawakami, and A. Scherer, Submicroscopic transient lens spectroscopy of InGaN/GaN quantum wells, Phys. Status Solidi (b) **240**, 368 (2003).

[3] J. Ma, D. Kuciauskas, D. Albin, R. Bhattacharya, M. Reese, T. Barnes, J. V. Li, T. Gessert, and S.-H. Wei, Dependence of the minority-carrier lifetime on the stoichiometry of CdTe using time-resolved photoluminescence and first-principles calculations, Phys. Rev. Lett. **111**, 067402 (2013).

[4] T. Suguhara, H. Sato, M. Hao, Y. Naoi, S. Kurai, S. Tottori, K. Yamashita, K. Nishino, L. T. Romano, and S. Sakai, Direct evidence that dislocations are non-radiative recombination centers in GaN, Jpn. J. Appl. Phys. **37**, L398 (1998).

[5] I. N. Krivorotov, T. Chang, G. D. Gilliland, L. P. Fu, and K. K. Bajaj, Exciton transport and nonradiative decay in semiconductor nanostructures, Phys. Rev. B **58**, 10687 (1998).

[6] Patrik Ščajev, Kęstutis Jarašiūnas, Serdal Okur, Ümit Özgür, and Hadis Morkoç, Carrier dynamics in bulk GaN, J. Appl. Phys. **111**, 023702 (2012); Ramūnas Aleksiejūnas, Patrik Ščajev, Saulius Nargelas, Tadas Malinauskas, Arūnas Kadys, and Kęstutis Jarašiūnas, Impact of diffusivity to carrier recombination rate in nitride semiconductors: from bulk GaN to (In, Ga)N quantum wells, Jpn. J. Appl. Phys. **52**, 08JK01 (2013).

[7] T. H. Gfroerer, C. M. Crowley, C. M. Read, and M. W. Wanlass, Excitation-dependent recombination and diffusion near an isolated dislocation in GaAs, J. Appl. Phys. **111**, 093712 (2012).

[8] T. H. Gfroerer, Yong Zhang, and M. W. Wanlass, An extended defect as a sensor for free carrier diffusion in a semiconductor, Appl. Phys. Lett. **102**, 012114 (2013).

[9] N. Armani, C. Ferrari, G. Salviati, F. Bissoli, M. Zha, A. Zappettini, and L. Zanotti, Defect-induced luminescence in high-resistivity high-purity undoped CdTe crystals, J. Phys. Condens. Matter **14**, 13203 (2002).

[10] P. Scajev, S. Nargelas, and K. Jarasiunas, Time-resolved free carrier lifetime microscopy in bulk GaN, Phys. Status Solidi RRL **7**, 647 (2013).

[11] J. Hassan and J. P. Bergman, Influence of structural defects on carrier lifetime in 4 H -SiC epitaxial layers: Optical lifetime mapping, J. Appl. Phys. **105**, 123518 (2009).

[12] M. J. DiNezza, X.-H. Zhao, S. Liu, A. P. Kirk, and Y.-H. Zhang, Growth, steady-state, and time-resolved photoluminescence study of CdTe/MgCdTe double heterostructures on InSb substrates using molecular beam epitaxy, Appl. Phys. Lett. **103**, 193901 (2013).

[13] K. Alberi, B. Fluegel, H. Moutinho, R. G. Dhere, J. V. Li, and A. Mascarenhas, Measuring long-range carrier diffusion across multiple grains in polycrystalline semiconductors by photoluminescence imaging, Nat. Commun. **4**, 2699 (2013).

[14] W. Stadler, D. M. Hofmann, H. C. Alt, T. Muschik, B. K. Meyer, E. Weigel, G. Müller-Vogt, M. Salk, E. Rupp, and K. W. Benz, Optical investigations of defects in $Cd_{1-x}Zn_xTe$, Phys. Rev. B **51**, 10619 (1995).

[15] L. M. Smith, D. R. Wake, J. P. Wolfe, D. Levi, M. V. Klein, J. Klem, T. Henderson, and H. Morkoç, Picosecond imaging of photoexcited carriers in quantum wells: Anomalous lateral confinement at high densities, Phys. Rev. B **38**, 5788 (1988).

[16] D. J. Wolford, G. D. Gilliland, T. F. Kuech, J. A. Bradley, and H. P. Hjalmarson, Optically determined minority-carrier transport in $GaAs/Al_xGa_{1-x}$ As heterostructures, Phys. Rev. B **47**, 15601 (1993).

[17] See Supplemental Material at http://link.aps.org/supplemental/10.1103/PhysRevApplied.2.034010 for the full range of images.

[18] N. M. Haegel, T. J. Mills, M. Talmadge, C. Scandrette, C. L. Frenzen, H. Yoon, C. M. Fetzer, and R. R. King, Direct imaging of anisotropic minority-carrier diffusion in ordered GaInP, J. Appl. Phys. **105**, 023711 (2009).

[19] In the DAP band, the acceptors involved can also be vacancy complexes known as A centers. S. Biernacki, U. Scherz, and B. K. Meyer, Electronic properties of A centers in CdTe: A comparison with experiment, Phys. Rev. B **48**, 11726 (1993).

[20] E. S. Barnard, E. T. Hoke, S. T. Connor, J. R. Groves, T. Kuykendall, Z. Yan, E. C. Samulon, E. D. Bourret-Courchesne, S. Aloni, P. J. Schuck, C. H. Peters, and B. E. Hardin, Probing carrier lifetimes in photovoltaic materials using subsurface two-photon microscopy, Sci. Rep. **3**, 2098 (2013).

[21] D. Kuciauskas, A. Kanevce, J. M. Burst, J. N. Duenow, R. Dhere, D. A. Albin, D. H. Levi, and R. K. Ahrenkiel, Minority carrier lifetime analysis in the bulk of thin-film absorbers using subbandgap (two-photon) excitation, IEEE J. Photovoltaics **3**, 1319 (2013).